Struct Multidisc Optim
DOI 10.1007/s00158-008-0323-7

INDUSTRIAL APPLICATION

Optimization of sonic crystal attenuation properties by *ev-MOGA* multiobjective evolutionary algorithm

J. M. Herrero · S. García-Nieto · X. Blasco · V. Romero-García · J. V. Sánchez-Pérez · L. M. Garcia-Raffi

Received: 3 March 2008 / Revised: 18 September 2008 / Accepted: 22 September 2008

Abstract This paper shows a promising method for acoustic barrier design using a new acoustic material called Sonic Crystals (SCs). The configuration of these SCs is set as a multiobjective optimization problem which is very difficult to solve with conventional optimization techniques. The paper presents a new parallel implementation of a Multiobjective Evolutionary Algorithm called *ev-MOGA* (also known as εMOGA) and its application in a complex design problem. *ev-MOGA* algorithm has been designed to converge towards a reduced, but well distributed, representation of the Pareto Front (solution of the multiobjective optimization problem). The algorithm is presented in detail and its most important properties are discussed. To reduce the *ev-MOGA* computational cost when objective functions are substantial, a basic parallelization has been implemented on a distributed platform.

Keywords Evolutionary multiobjective optimization · Sonic cristals · Parallel MOEA · Acoustic attenuation

1 Introduction

Noise control has long been considered a standard topic in science and technology. There are three phases at which noise can be controlled: in the generation (source of noise), in the transmission (from the source to the receiver) and in the reception (receiver of noise). The use of acoustic barriers is the most suitable method for controlling the noise in the transmission step.

The acoustic effect of barriers can be explained as follows: the transmitted noise travels from the source to the receiver in a straight line. This path is interrupted by an acoustic barrier situated between the source and the receiver. A portion of the transmitted acoustic energy is reflected or scattered back towards the source, and another portion is transmitted through the barrier, diffracted at the top edge or absorbed by the material of the barrier. Thus, as one can see in Fig. 1, the receiver is exposed to the transmitted and diffracted noise. Transmission depends on the barrier's material properties and refraction depends on the dimensions, location, and shape of the barrier. Acoustic design considerations include aspects regarding the material, location, dimensions, and shape of the barrier.

In last decade new acoustic materials called sonic crystals (SCs) have been developed (Martínez-Sala et al. 1995; Sánchez-Pérez et al. 1998; Kushwaha 1997;

Partially supported by MEC (Spanish Government) and FEDER funds: projects DPI2005-07835, MAT2006-03097 and Generalitat Valenciana (Spain) projects GV06/026, GV/2007/191.

J. M. Herrero · S. García-Nieto · X. Blasco (✉)
Department of Systems Engineering and Control, Polytechnic University of Valencia, Camino de vera s/n, 46022 Valencia, Spain
e-mail: xblasco@isa.upv.es

V. Romero-García · J. V. Sánchez-Pérez
Centro de Tecnologías Físicas, Polytechnic University of Valencia, Camino de Vera s/n, 46022 Valencia, Spain

L. M. Garcia-Raffi
Instituto Universitario de Matemática Pura y Aplicada, Polytechnic University of Valencia, Camino de Vera s/n, 46022 Valencia, Spain

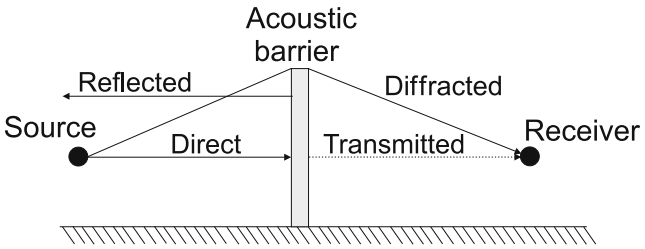

Fig. 1 Acoustic effect of a barrier

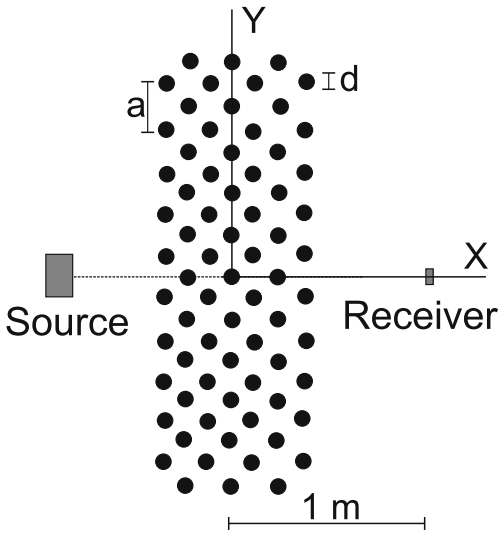

Fig. 3 Transversal scheme of an SC formed by isolated cylinders in a triangular array used as an acoustic barrier. '*a*' represents the lattice constant of the array, and '*d*' is the cylinder diameter

Shen and Cao 2001; Cervera et al. 2002), which can be presented as an alternative to classic acoustic barriers. These materials consist of periodic distributions of acoustic scatterers in another medium with different physical properties. These composite materials have an important acoustic characteristic related with the attenuation of sound: they contain spectral band gaps that prevent the propagation of sound in a predetermined range of frequencies, depending both on the periodicity of the array formed and on the configuration of the unit cell. Specifically, some authors (Sánchez-Pérez et al. 2002) have demonstrated the possibility of using 2D SCs formed with isolated cylindrical scatterers made with rigid materials to construct acoustic barriers (Fig. 2).

The use of these materials as acoustic attenuation devices is advantageous because they can be installed without foundations. This is because their structure allows air to pass through them, so reducing the air pressure on the SC barrier. Nevertheless, their technological use must be developed in order to solve the acoustical disadvantages they present compared to classical barriers. The main problem is the creation of large attenuation bands for wide ranges of frequencies - because the size of an attenuation band depends on both the physical characteristics of the cylindrical scatterers and on their positioning. Specifically, the number, size, and lattice constant, of the cylinders arrays must be taken into account (Fig. 3). In other words, the attenuation peaks widen when we increase the number and diameter of the cylinders and, moreover, the position of an attenuation band in the frequency spectrum depends on the distance between cylinders. Obtaining an optimum arrangement of cylinders to ensure the best acoustic attenuation is not a trivial problem.

All of these physical arguments, together with the complexity of the mathematical functions involved in the attenuation SC calculus, indicate that SCs are suitable for using optimization algorithms to improve their attenuation capability. In fact, some researchers have used genetic algorithms (GA) in order to optimize the lens behaviour of these materials, by varying the diameter and the position of the cylinders, and creating vacancies in the starting SC (Hakkansson et al. 2005; Sanchis et al. 2004). Other research groups have used GA as a strategy to enhance the acoustic properties of the SCs (Hussien et al. 2006, 2007; Gazonas et al. 2006). Specifically, the attenuation capability of the SCs can be improved by creating vacancies in the cylinder array (Romero-García et al. 2006).

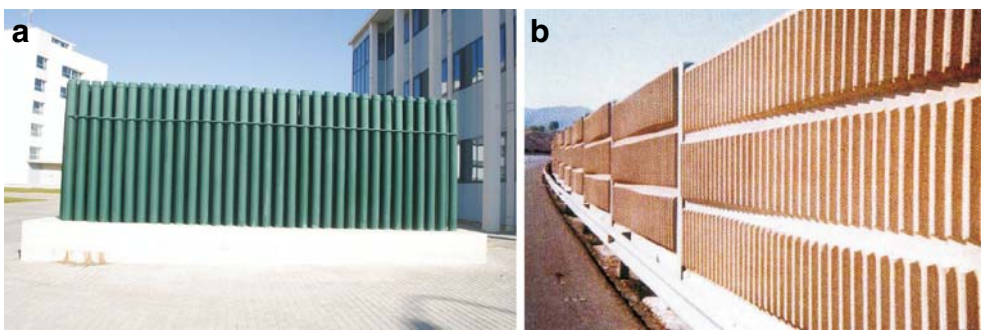

Fig. 2 **a** SC used as acoustic barrier; **b** Classical acoustic barrier

The physical problem to solve is how to optimize the attenuation properties of SCs by creating vacancies in the starting and complete SC. Acoustically, this means: (*i*) maximize the attenuation level in a predetermined wide frequency range, and (*ii*) minimize deviation from the average attenuation value within the predetermined frequency range. Until now, all previous work has attempted to find optimal SCs by formulating the problem as a single objective optimization problem. However, we propose improving the solution by reformulating the problem as a multiobjective problem (MOP).

The problem is very complex and has a high computational cost—requiring new optimization algorithms to solve it. One interesting alternative in resolving MOPs is based on the use of evolutionary algorithms (EAs)—allowing several elements of the Pareto optimal set to be generated at the same time, in parallel and in a single run. This is made possible thanks to the populational nature of EAs. A number of authors have developed different operators, or strategies, for converting the original EAs into multiobjective optimization evolutionary algorithms (MOEAs) that converge towards the Pareto optimal set and are diverse enough to be able to characterize it. The good results obtained with MOEAs, together with their capacity to handle a wide variety of problems with different degrees of complexity, explains why they are being used more frequently. Indeed, they are currently one of the branches where the most progress is being made within the field of EAs. (Fonseca 1995; Zitzler 1999; Coello et al. 2002, 2005; Alander 2002).

This article shows a new parallel implementation of a multiobjective optimization algorithm (*ev-MOGA*) and its application in the improvement of the attenuation properties of SCs. Different strategies for creating the vacancies have been used because of the problem complexity: X symmetry, Y symmetry, X plus Y symmetry, and random. Throughout this work, we have considered 2D SCs made with an array of cylinders surrounded by air.

2 Theoretical considerations

2.1 Multiple scattering theory

Analysis of sound propagation in periodic structures such as SCs needs the use of mathematical methods. In recent years some authors have developed several tools to reproduce the acoustic behaviour of SCs. These methods can be classified as either theoretical and phenomenological. The theoretical methods are based either on mathematical functions with fixed symmetry, or on numerical resolution of the wave equation (Chen and Ye 2001; García-Pablos et al. 2000). Phenomenological methods are based on experimental data obtained in specific experimental situations (Fuster et al. 2006).

Several modelling methods have been developed—depending on the characteristics of the SCs analyzed. The Plane-wave (PW) method (Sigalas and Economou 1992) is a powerful technique, but it presents convergence problems in some special cases, for example, periodic (or non-periodic) structures with large density contrasts in the physical properties between the scatterers and host material. These difficulties can be reduced if we use a Multiple Scattering (MS) method. For this situation, Multiple Scattering Theory (MST) seems more numerically efficient than the PW method.

The physical mechanism of this method can be explained as follows: when sound is propagated through a medium with many scatterers, waves are scattered by each scatter. Acoustic waves may be scattered yet again by other scatterers. This phenomenon is repeated infinitely to establish a multiple scattering process. The MST (Chen and Ye 2001; Kafesaki and Economou 1999), based on the well known Korringa-Kohn-Rostoker theory (KKR) (Korringa 1947; Kohn and Rostoker 1954), is a self-consistent method for calculating acoustic pressure, including all orders of scattering for mixed composites and for high-contrast composites. Moreover, with this method we can calculate transmission through finite arrays of these composites.

In this work, the simulation of the sound scattered by each analyzed structure will be performed by a two-dimensional (2D) MST. If we consider the pressure and normal continuous velocity across the interface between a scatterer and the surrounding medium, the acoustic pressure at any point outside all the cylinders can be expressed by

$$P(\vec{r}) = i\pi H_0^{(1)}(k|\vec{r}|) + \\ + \sum_{l=1}^{N} \sum_{q=-\infty}^{q=\infty} i\pi A_{lq} H_{lq}^{(1)}(k|\vec{r} - \vec{r}_l|) \exp(iq\phi_{\vec{r}-\vec{r}_l}), \tag{1}$$

where N is the number of cylinders with radius r located at r_l (with $l = 1, ..., N$), k is the wave number, i is the imaginary unit, $H_0^{(1)}$ is the 0-th order first kind Hankel function and $\phi_{\vec{r}-\vec{r}_l}$ is the azimuthal angle of the vector $\vec{r} - \vec{r}_l$ to the positive x-axis. A_{lq} are the coefficients of the series expansion of the pressure, and H_{lq} is the q-th order first kind Hankel function.

2.2 Complexity and objectives

There are several reasons why classical optimization methods are difficult to use in the problems presented in this work: the type of dependencies, the dimension of the search space, and the computational time.

The coefficients of the series expansions in the MST, A_{lq}, which are determined numerically from the equations obtained by means of the boundary conditions, depend on the parameters defining the crystal, and on the frequency. As a consequence, the acoustic pressure, (1), depends simultaneously on discrete and continuous variables. Therefore, (1) is difficult to optimize.

The dimension of the search space in optimization methods is an important parameter to take into account. The larger the search space, the more difficult the resulting optimization problem. In this work, the dimension of the search space is large due to the great number of variables involved in the MST.

Finally, the computational time to calculate A_{lq} increases to the third power of the number of cylinders, N^3, so large numbers of cylinders implies a high computational time. The use of SCs as acoustic barriers means structures with many scatterers, and this again indicates the complexity of the problem.

The objectives used in this paper are based on the acoustic attenuation properties of an array of scatterers. The theoretical acoustic attenuation at a point (x, y), for an incidence frequency ν and an array of cylinders of radius r_l placed at (X_{cyl}, Y_{cyl}) coordinates is:

$$Attenuation(dB) = 20 \log \frac{|P_{direct}(x, y)|}{|P_{interfered}(x, y, X_{cyl}, Y_{cyl}, \nu, r_l)|} \quad (2)$$

where the interfered pressure is determined by the MST, (1). And X_{cyl}, Y_{cyl} represent the x and y coordinates of cylinders that form the array of scatterers.

To maximize the sound attenuation in a predetermined range of frequencies at a point of coordinates (x, y) two objective functions are defined, setting the problem as a multiobjective,

$$J_1(\boldsymbol{\theta}) = \bar{p} = \sum_{j=1}^{N_\nu} \frac{|p_j(\boldsymbol{\theta})|}{N_\nu} \quad (3)$$

$$J_2(\boldsymbol{\theta}) = \sqrt{\frac{\sum_{j=1}^{N_\nu} (\bar{p} - |p_j(\boldsymbol{\theta})|)^2}{N_\nu^2}} \quad (4)$$

where N_ν represents the number of frequencies considered in this range and $\boldsymbol{\theta}$ is a vector that contains the information about the space configuration of the structure.

$J_1(\boldsymbol{\theta})$ represents the mean pressure in the range of frequencies $[\nu_1 = 2300, \nu_N = 3700]Hz$, and $J_2(\boldsymbol{\theta})$ represents the mean deviation. In our case, we use $N_\nu = 29$, meaning $\triangle\nu = 50Hz$. The design variable under study $\boldsymbol{\theta}$ is a vector that indicates the existence, or not, of a cylinder in each position of the SC.

2.3 Analyzed structures

The base SC structure (see Fig. 3) is made of 73 cylinders located in 7 rows, in a triangular array which lattice constant of $6.35cm$.

The optimized structures are obtained by means of the creation of vacancies by removing cylinders in the base SC structure. Thus, we analyze the search space by varying the design variable, $\boldsymbol{\theta}$.

In this work, several rules to create vacancies in the starting SC have been analyzed: (*a*) symmetry around the X axes, (*b*) symmetry around the Y axes, (*c*) symmetry around both the X and Y axes, and (*d*) no symmetry (random). Figure 4 shows an example of each symmetry used.

The design variable is a vector (chromosome) whose coordinates (genes) represent the existence, or not, of a cylinder in a specific position of the starting SC. Each gene is related with the coordinates of a scatterer of the starting SC. Every possible position of a cylinder in the SC is localized with a matrix of positions (X_{cyl}, Y_{cyl}). In this problem, the matrix has 73 rows and two columns (the first column represents x position and the second column represents y position). So the i–gene is related with the i–row in matrix (X_{cyl}, Y_{cyl}). The value in each gene of the design variable $\boldsymbol{\theta}$ can vary in the [0, 1] range. A gene with a value in]0.5, 1] represents the existence of a cylinder in the position associated with it, and a value in $[0, 0.5]$ means the existence of a vacancy at this position.

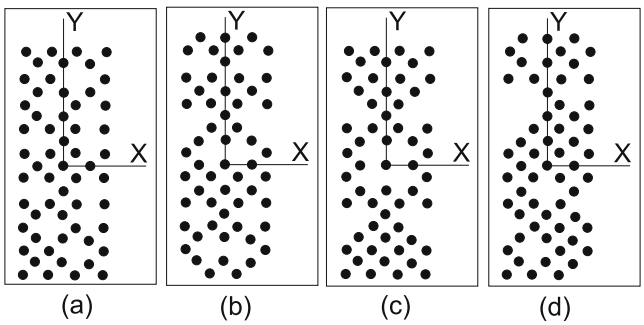

Fig. 4 Creation of vacancies in an SC; **a** X symmetry; **b** Y symmetry; **c** X plus Y symmetry; **d** no symmetry constraints

If symmetric vacancies are analyzed, the chromosome only presents the genes corresponding to the positions of the symmetric part of the SC, and to obtain the complete chromosome, a mirror image of this coordinate is made. This methodology ensures that cylinder location are not overlapped.

2.4 Multiobjective evolutionary algorithm

The $\epsilon-$MOGA variable (*ev-MOGA*) is an elitist multiobjective evolutionary algorithm based on the concept of $\epsilon-$dominance (Laumanns et al. 2002).

With regard to MOP, a completed and detailed version of the *ev-MOGA* algorithm is developed in Herrero (2006) where the algorithm is compared with the $\epsilon-$MOEA (Mishra et al. 2005) by means of a set of five classical benchmarks for MOPs (MOP1 to MOP5 extract from Coello et al. (2002)). $\epsilon-$MOEA algorithm is also based on the concept of $\epsilon-$dominance. In Mishra et al. (2005), a comparison between the $\epsilon-$MOEA and other well known algorithms such as NSGA-II, PESA, SPEA2, etc. shows the superiority of the $\epsilon-$MOEA. As stated in Deb (2007), $\epsilon-$MOEA is computationally faster and achieves better distributed solutions than NSGA-II or SPEA2.

Generally, the *ev-MOGA* algorithm presents better values for classical MO metrics (Pareto solutions (PS) generational distance (GD), hyperarea ratio (HR), spacing (SP) and box ratio BR[1]) as shown in Table 1. The algorithms optimize each problem ten times with a different initial population (randomly created) and the average values for each metric are shown in this table.

ev-MOGA obtains an $\epsilon-$Pareto set, $\hat{\Theta}_P^*$, that converges towards the Pareto optimal set Θ_P in a distributed way and utilizes limited memory resources. Another difference with $\epsilon-$MOEA is that *ev-MOGA* is able to adjust the limits of the Pareto front dynamically and prevent solutions belonging to the extremes of the front from being lost.

The objective function space is split into a fixed number of boxes forming a grid. For each dimension, n_box_i cells of ϵ_i width calculated as

$$\epsilon_i = \left(J_i^{max} - J_i^{min}\right)/n\_box_i \tag{5}$$

This grid preserves the diversity of $\boldsymbol{J}(\hat{\Theta}_P^*)$ since one box can be occupied by only one solution. This fact prevents the algorithm from converging towards just one point or area inside the function space (Fig. 5).

[1]For more details about these metrics see Coello et al. (2002).

Table 1 Comparative values of the PS, GD, HR, SP and BR metrics for the MOP1 to MOP5 problems between *ev-MOGA* and $\epsilon-$MOEA algorithm

	PS	GD	HR	SP	BR
MOP1					
ev-MOGA	**25**	**0.00292**	**0.929**	0.00767	**0.5145**
$\epsilon-$MOEA	**25**	0.00296	**0.929**	**0.00765**	0.5143
MOP2					
ev-MOGA	**42**	**0.00101**	**0.981**	**9.625e-7**	**0.9223**
$\epsilon-$MOEA	**42**	0.00107	0.9798	4.676e-6	0.883
MOP3					
ev-MOGA	**39.8**	**0.0158**	**0.9605**	**0.0632**	**0.8379**
$\epsilon-$MOEA	38.8	0.0222	0.9603	0.0658	0.8374
MOP4					
ev-MOGA	**53**	**0.00299**	**0.9803**	**0.0118**	**0.938**
$\epsilon-$MOEA	49.7	0.00309	0.975	0.0168	0.9323
MOP5					
ev-MOGA	**53.6**	**0.00364**		**0.0182**	0.6057
$\epsilon-$MOEA	30.6	0.00531		0.02818	**0.6412**

Bold numbers show the better values obtained for each metric and problem

The concept of $\epsilon-$dominance is defined as follows. For a model $\boldsymbol{\theta}$, $box_i(\boldsymbol{\theta})$ is defined by

$$box_i(\boldsymbol{\theta}) = \left\lceil \frac{J_i(\boldsymbol{\theta}) - J_i^{min}}{J_i^{max} - J_i^{min}} \cdot n\_box_i \right\rceil \; \forall i \in [1 \ldots s] \tag{6}$$

Let $\boldsymbol{box}(\boldsymbol{\theta}) = \{box_1(\boldsymbol{\theta}), \ldots, box_s(\boldsymbol{\theta})\}$. A solution vector $\boldsymbol{\theta}^1$ with function value $\boldsymbol{J}(\boldsymbol{\theta}^1)$ $\epsilon-$dominates the vector $\boldsymbol{\theta}^2$ with function value $\boldsymbol{J}(\boldsymbol{\theta}^2)$, denoted by:

$$\boldsymbol{J}(\boldsymbol{\theta}^1) \prec_\epsilon \boldsymbol{J}(\boldsymbol{\theta}^2), \tag{7}$$

if and only if:

$$\left(\boldsymbol{box}(\boldsymbol{\theta}^1) \prec \boldsymbol{box}(\boldsymbol{\theta}^2)\right) \vee \\ \vee \left(\left(\boldsymbol{box}(\boldsymbol{\theta}^1) = \boldsymbol{box}(\boldsymbol{\theta}^2)\right) \wedge \left(\boldsymbol{J}(\boldsymbol{\theta}^1) \prec \boldsymbol{J}(\boldsymbol{\theta}^2)\right)\right). \tag{8}$$

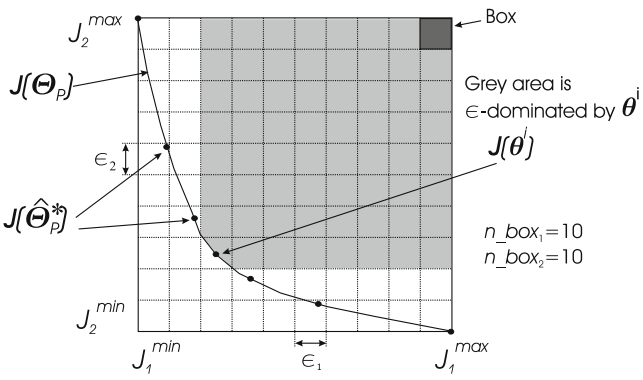

Fig. 5 The concept of $\epsilon-$dominance. $\epsilon-$Pareto Front $\boldsymbol{J}(\hat{\Theta}_P^*)$ in a two-dimensional problem. J_1^{min}, J_2^{min}, J_1^{max}, J_2^{max}, limits space; ϵ_1, ϵ_2 box widths; and n_box_1, n_box_2, number of boxes for each dimension

Hence, a set $\hat{\Theta}_P^*$ is $\epsilon-$Pareto if and only if $\forall \boldsymbol{\theta}^1, \boldsymbol{\theta}^2 \in \hat{\Theta}_P^*,\ \boldsymbol{\theta}^1 \neq \boldsymbol{\theta}^2$

$$\hat{\Theta}_P^* \subseteq \Theta_P \wedge (\boldsymbol{box}(\boldsymbol{\theta}^1) \neq \boldsymbol{box}(\boldsymbol{\theta}^2)) \tag{9}$$

Next, the procedure to obtain an $\epsilon-$Pareto front $\boldsymbol{J}(\hat{\Theta}_P^*)$, which is a well-distributed approximation sample of the Pareto front $\boldsymbol{J}(\Theta_P)$, is described. The algorithm, which adjusts the width $\epsilon_\mathbf{i}$ dynamically, is composed of three populations (see Fig. 6).

1. Main population $P(t)$ explores the searching space D during the algorithm iterations (t). Population size is $Nind_P$.
2. Archive $A(t)$ stores the solution $\hat{\Theta}_P^*$. Its size $Nind_A$ can be variable and will never be greater than

$$Nind\_max\_A = \frac{\prod_{i=1}^{s}(n\_box_i + 1)}{n\_box_{max} + 1} \tag{10}$$

   where $n\_box_{max} = \max_i n\_box_i$.
3. Auxiliary population $G(t)$. Its size is $Nind_G$, which must be an even number.

The pseudocode of the *ev-MOGA* algorithm is given by

```
1.   t:=0
2.   A(t):=∅
3.   P(t):=ini_random(D)
4.   eval(P(t))
5.   A(t):=store_ini(P(t),A(t))
6.   while t<t_max do
7.        G(t):=create(P(t),A(t))
8.        eval(G(t))
9.        A(t+1):=store(G(t),A(t))
10.      P(t+1):=update(G(t),P(t))
11.      t:=t+1
12.  end while
```

The main steps of the algorithm are briefly detailed as follows:[2]

Step three. $P(0)$ is randomly initialized with $Nind_P$ individuals (design vectors $\boldsymbol{\theta}$).

Step four and eight. Function **eval** calculates function values (equations (3) and (4)) for each individual in $P(t)$ (step four) and $G(t)$ (step eight).

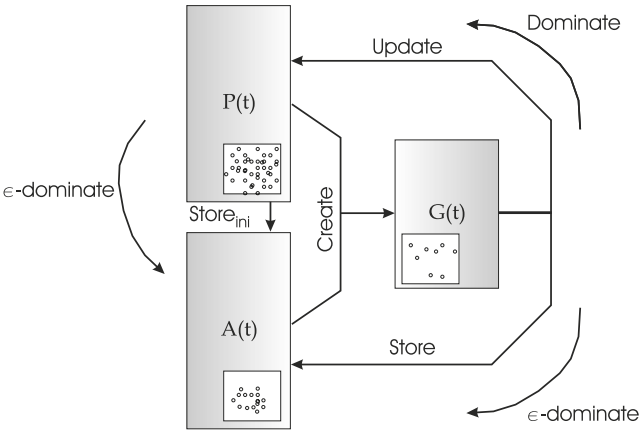

Fig. 6 *ev-MOGA* algorithm structure. $P(t)$, the main population; $A(t)$, the archive; $G(t)$ the auxiliary population

Step five. Function **store**$_{ini}$ checks individuals of $P(t)$ that might be included in the archive $A(t)$ as follows:

a. Non-dominated $P(t)$ individuals are detected, Θ_{ND}.
b. Function space limits are calculated from $\boldsymbol{J}(\Theta_{ND})$.
c. Individuals in Θ_{ND} that are not $\epsilon-$dominated will be included in $A(t)$.

Step seven. Function **create** creates $G(t)$ by means of crossover (extended linear recombination technique) and mutation (using random mutation with Gaussian distribution) operators.

Step nine. Function **store** checks which individuals in $G(t)$ must be included in $A(t)$ on the basis of their location in the function space (see Fig. 7). Thus $\forall \boldsymbol{\theta}^G \in G(t)$

a. If $\boldsymbol{\theta}^G$ lies in the area $Z1$ and is not $\epsilon-$dominated by any individual from $A(t)$, it will be included in $A(t)$. Individuals from $A(t)$ which are $\epsilon-$dominated by $\boldsymbol{\theta}^G$ will be eliminated.
b. If $\boldsymbol{\theta}^G$ lies in the area $Z2$ then it is not included in the archive, since it is dominated by all individuals in $A(t)$.
c. If $\boldsymbol{\theta}^G$ lies in the area $Z3$, the same procedure is applied as was used with the function **store**$_{ini}$ but now applied over the population $P'(t) = A(t) \bigcup \boldsymbol{\theta}^G$.

[2] A more detailed description can be obtained in Herrero et al. (2007).

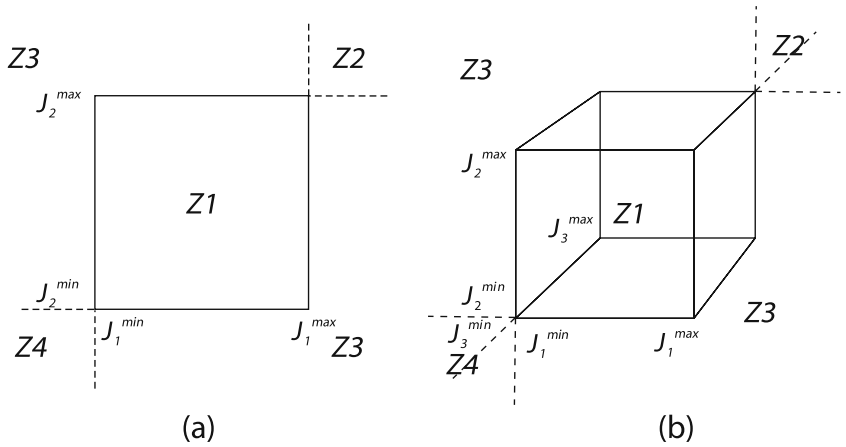

Fig. 7 Objective function space areas (Z) and limits ($\boldsymbol{J}$). Showing **a** two-dimensional case **b** three-dimensional case

In this procedure, new function limits and ϵ_i widths could be recalculated.

d. If $\boldsymbol{\theta}^G$ lies in the area $Z4$, all individuals from $A(t)$ are deleted since they are all $\epsilon-$dominated by $\boldsymbol{\theta}^G$. $\boldsymbol{\theta}^G$ is included and function space limits are $\boldsymbol{J}(\boldsymbol{\theta}^G)$.

Step 10. Function **update** updates $P(t)$ with individuals from $G(t)$. Every individual $\boldsymbol{\theta}^G$ from $G(t)$ replaces an individual $\boldsymbol{\theta}^P$ that is randomly selected from among the individuals in $P(t)$ that are dominated by $\boldsymbol{\theta}^G$. $\boldsymbol{\theta}^P$ will not be included in $P(t)$ if there is no individual in $P(t)$ dominated by $\boldsymbol{\theta}^G$.

Finally, individuals from $A(t)$ compound the solution $\hat{\Theta}_P^*$ of the multiobjective optimization problem.

2.5 Parallelization

The high computational cost of the SC attenuation property optimization problem produces huge execution times, i.e. average execution time for a population $P(t)$ of 120 individuals, population $G(t)$ of 8, and $t_{max} = 6500$ generations is around 417035 s[3] (4 days, 19 h, 50 min and 35 s). Improvements of execution time have been obtained with a parallel implementation of the *ev-MOGA* described. Several alternative for parallelization are possible (Cantú-Paz 1997) the Master-Slave configuration being selected. For this architecture, there is one processor working as Master, executing tasks of the *ev-MOGA*, and the rest evaluate the fitness function of a subpopulation (see Fig. 8).

The Master has to send a subpopulation to each Slave, who makes a fitness evaluation and returns results to the Master. The Master works in a synchronous way, waiting for all fitness values from all the Slaves. After receiving all the fitness values the Master performs the evolution to produce the next iteration and sends to the Slaves the new population for fitness evaluation. This type of implementation is the simplest and does not change *ev-MOGA* operators and behaviour. The time reduction is significant since the overall time is theoretically divided by the number of Slaves—if the evolution procedure and Master-Slave communication tasks have no computational cost. With the proposed implementation, the evolution cost is important and the theoretical reduction is not achieved. Even then, the time saving is quite large, for the proposed problem, with eight Slaves, the total execution is reduced to 104204 s (1 day, 4 h, 56 min and 44 s).

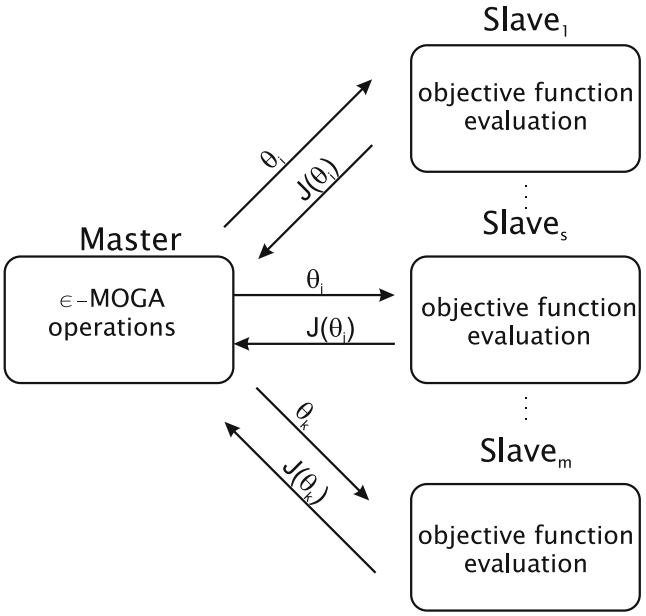

Fig. 8 Master/Slave architecture for *ev-MOGA*

[3]Execution is performed with one of the computers on the distributed platform described later.

The distributed platform is built with eight computers as described:

- All computers are Intel® Pentium® D 3.4 GHz.
- The master computer has 2 GB RAM and the operating system is Windows Server 2003. This computer works as master and has one slave.
- Slave computers have 1 GB RAM and Windows XP.
- Local network with Gigabit Ethernet.

All developments (*ev-MOGA* and SC models) have been made in Matlab®, parallelization has been performed with Matlab Distributed Computing Toolbox and Matlab Distributed Computing Engine.

3 Results

Multiple execution of the algorithm has been performed to increase the reliability of the results. The executions started with different constraints and initial populations. An increasing SC structure complexity policy is selected (Fig. 4)—the three first run constraints to solutions with SC symmetry in both axes, X symmetry plus Y symmetry; the next six run constraints only in one axis, three with X symmetry and three with Y symmetry. The final three executions impose no symmetry restriction. The computational complexity is lower when symmetry constraints are imposed—as no symmetry restriction means more complex calculus.

To improve results in each execution, the following procedure is followed:

- **symxy**: X plus Y symmetry and random initial population.
- **symxy2**: X plus Y symmetry and the solution of symxy solution is included in the initial population, the rest of the population is generated randomly.
- **symxy3**: X plus Y symmetry and the solution of symxy and symxy2 solutions are included in the initial population, the rest of the population is generated randomly.
- **symy**: Y symmetry and random initial population.
- **symy2**: Y symmetry and the solution of symy and symxy3 solutions are included in the initial population, the rest of the population is generated randomly.
- **symy3**: Y symmetry and the solution of symy2 solution is included in the initial population, the rest of the population is generated randomly.
- **symx**: X symmetry and random initial population.
- **symx2**: X symmetry and the solution of symx and symxy3 solutions are included in the initial population, the rest of the population is generated randomly.
- **symx3**: X symmetry and the solution of symx2 solution is included in the initial population, the rest of the population is generated randomly.
- **nosym**: Without symmetry constraint and random initial population.
- **nosym2**: Without symmetry constraint and the solution of nosym, symy3, symx3 and symxy3 solutions are included in the initial population, the rest of the population is generated randomly.
- **nosym3**: Without symmetry constraint and the solution of nosym2 solution is included in the initial population, the rest of the population is generated randomly.

The fact that each problem is executed several times with the best solutions of the previous runs is a common technique to prevent early exhaustion when the population diversity drops below a threshold. In the literature it is known as 'restart and phase', for instance, see CHC algorithm (Eshelman 1991). The three runs of the algorithm can be understood as a unique run with a mechanism of 'restart and phase'. When the algorithm is exhausted, it is restarted with a new population that includes the best individuals.

Figure 9 shows the best results for all symmetries and the relative position compared with ideal point. The ideal point is the one with the best value for each objective (Miettinen 1998). This point is not feasible, but the distance to this point is a classical index of quality (tradeoff between objectives) of the solution in a multiobjective optimization problem. In this example,

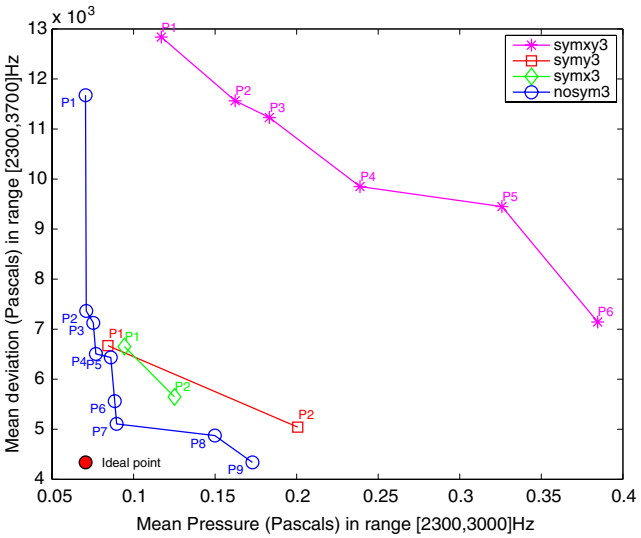

Fig. 9 Comparison of the best result for each symmetry constraint

the ideal point is formed by the best attenuation and mean deviation obtained with the best values of points P1 (which minimize mean pressure in a single objective sense) and P9 (which minimize mean desviation in a single objective sense) of nosym3 Pareto Front. This point is not achievable; but gives an order of magnitude of the best performances attainable. As can be seen, execution without symmetry constraints presents the best results because the structure has more flexibility. Y symmetry and X symmetry offer similar results. The worst results are for XY symmetry—due to the limited degree of freedom in the creation of vacancies.

Figures 10, 11, 12 and 13 show attenuation supplied by some of the points of the Pareto front obtained in the optimization phase, the points are labelled as P1, P2, etc. (see Fig. 9) in decreasing order of mean attenuation. For the fronts of more than two points, such as nosym3 and symxy3, for simplicity's sake and without loss of generality, only the extremes of the front and the nearest point to the ideal are considered for the next analysis.

Figure 10 represents the results of points P1, P4 and P6 of the Pareto front of symxy3. P1 has the best mean attenuation in the range of optimization ([2300, 3700] Hz) and P6 the best mean deviation in the same range; P4 is an intermediate solution between P1 and P6, and the nearest to the ideal point. An interesting characteristic is that P1 has the worst mean deviation, but when observing the frequency diagram of attenuation this is seen not to be a drawback because the larger variations in attenuation are in a positive sense and this behavior is favourable for the main objective. In essence, the objective is to obtain a high attenuation and all variations in this sense are positive. Even with a higher variation in attenuation with respect to P4 and P6, the attenuation for nearly every frequency in the range of interest is normally above the values of P4 and P6. Then a good solution for a final choice with XY symmetry is point P1.

Figure 11 represents the results of points P1 and P2 of symx3, in this case the complete Pareto front obtained in the optimization process. P1 has the best mean attenuation in the range of optimization ([2300, 3700] Hz) and P2 the best mean deviation in the same range. In both cases, the mean attenuation is quite similar. The deviation analysis in the optimization range reproduces similar characteristics as in the case symxy3. The higher deviation of P1 is not a drawback because the main deviation are in a positive sense. Again, a good choice for a final solution can be point P1.

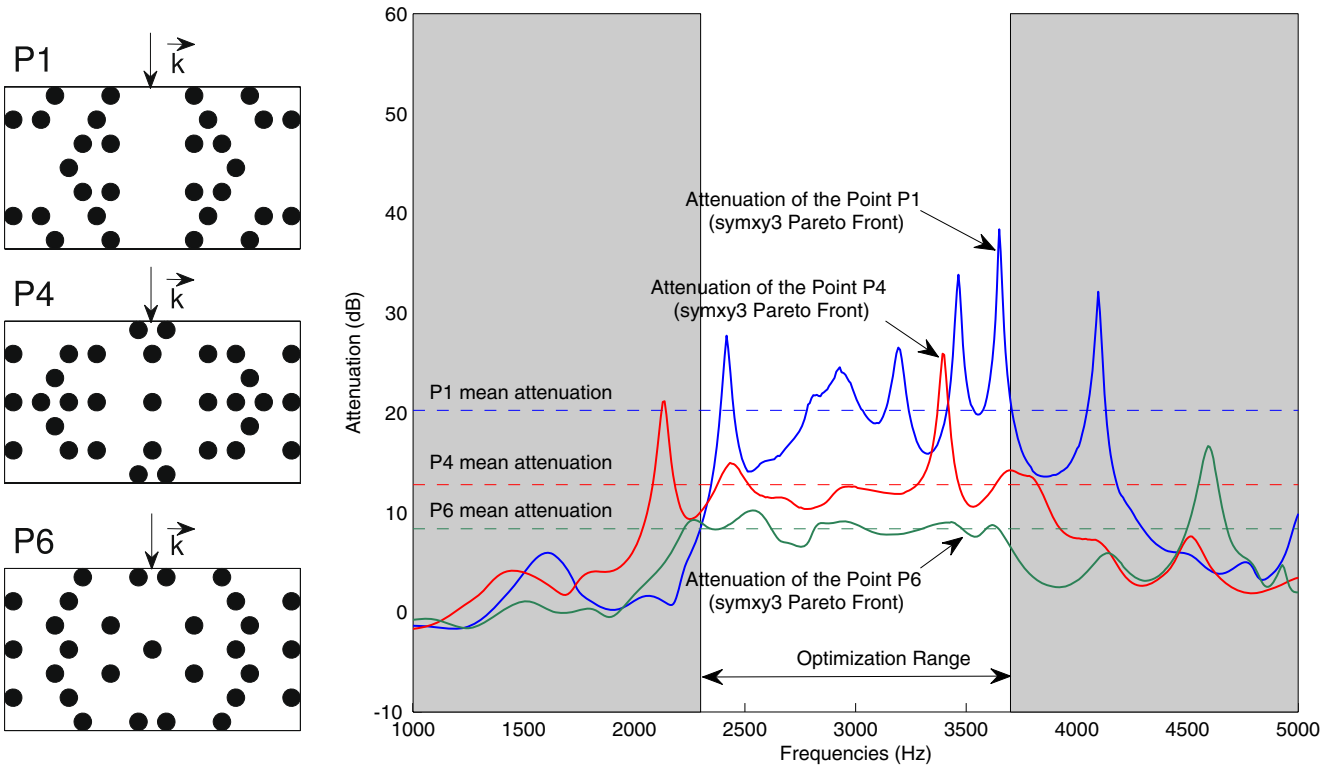

Fig. 10 Attenuations for points P1, P4, and P6 of the Pareto front symxy3. Mean attenuations have been calculated in ranges [2300, 3700] Hz

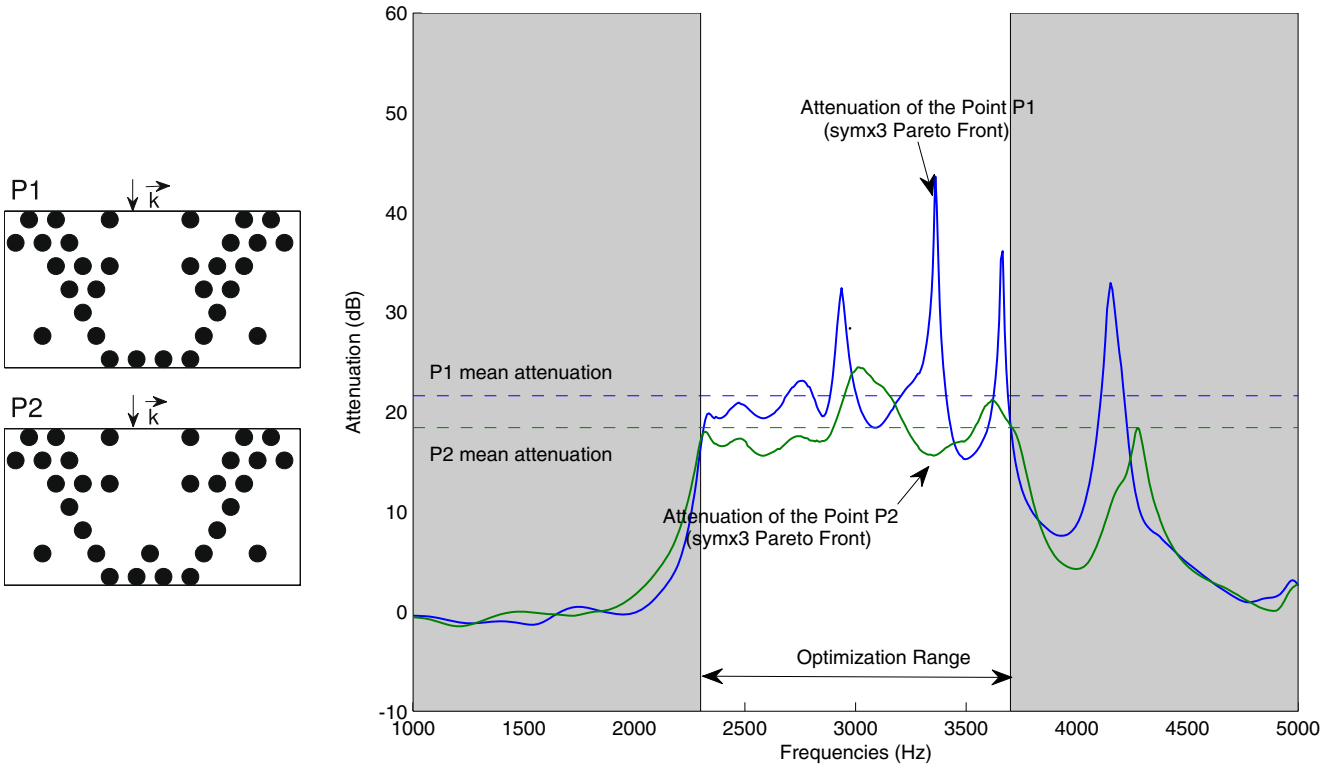

Fig. 11 Attenuations for points P1 and P2 of the Pareto front symx3. Mean attenuations have been calculated in ranges [2300, 3700] Hz

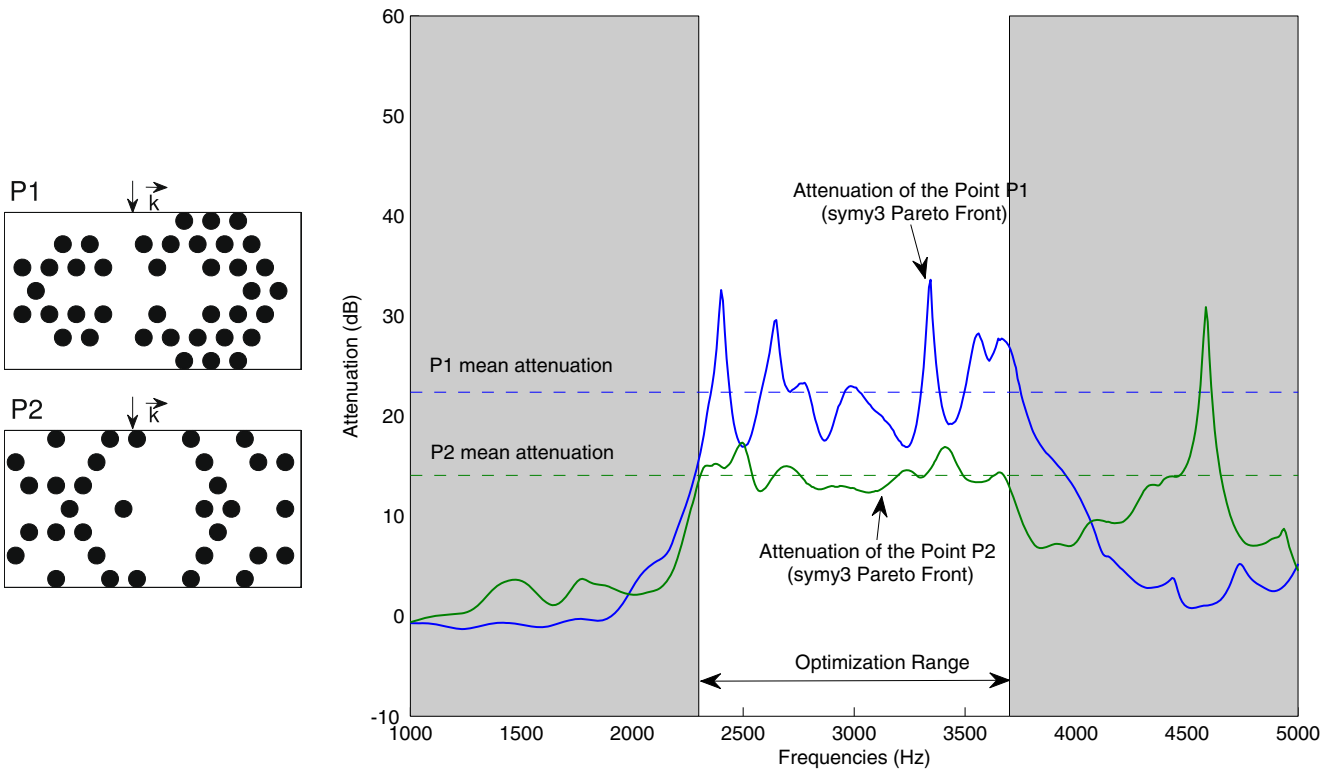

Fig. 12 Attenuations for points P1, P4 and P6 of the Pareto front symy3. Mean attenuations have been calculated in ranges [2300, 3700] Hz

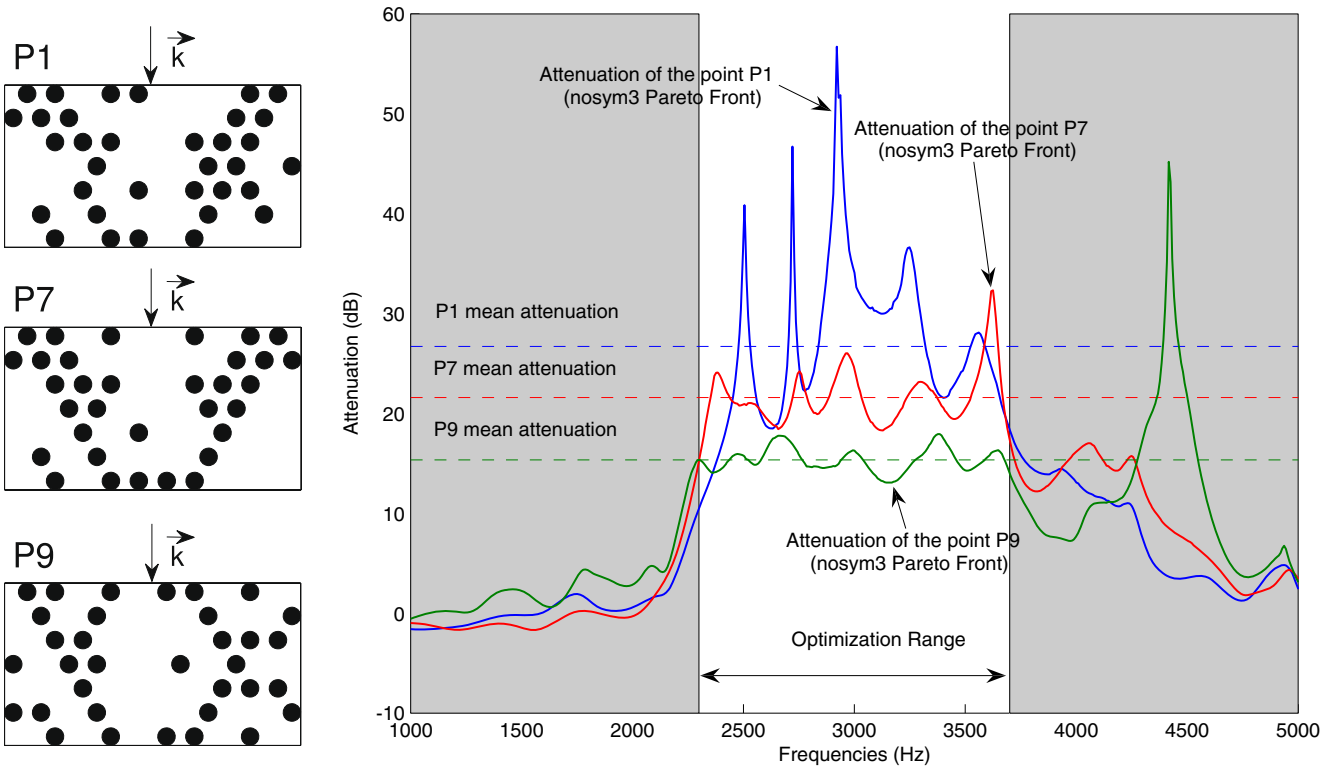

Fig. 13 Attenuations for points P1, P7 and P9 of the Pareto front nosym3. Mean attenuations have been calculated in ranges [2300, 3700] Hz

For results of Fig. 12 the analysis is quite similar to the previous one and the best choice for a final solution with Y symmetry is P1.

Figure 13 represents the results of points P1, P7, and P9 of the Pareto front of nosym3. P1 has the best mean attenuation in the range of optimization ([2300, 3700] Hz) and P9 the best mean deviation in the same range, P7 (the nearest to the ideal point) is an intermediate solution between P1 and P9. The analysis of XY, X, and Y symmetries shows an important characteristic in all symmetries: those responses with high deviations are not necessarily the worst—because the higher deviations are mostly in a positive sense which is good for higher attenuation. A good choice for a final solution could be P1 point. Moreover, this solution can be the best choice for all symmetries because it obtains the best mean attenuation.

A conclusion of this initial analysis is that the mean deviation seems to be less important than initially supposed in all solutions, and the higher deviation is not a drawback because it is in a positive sense. Two solutions could have the same mean attenuation but different deviations, in this case it is intuitively better to say that the lower deviation is better; and for this reason it is, a priori, a relevant quality indicator. But the results show that high deviations are mostly produced by high positive attenuation peaks (this phenomenon was not predicted, as positive and negative peaks with similar magnitudes were expected) while under average peaks of attenuation are less sharp. The positive peaks do not reduce the quality of attenuation: they increase the mean, but unfortunately, they also increase the deviation.

Therefore, future methodologies for the improvement of the SC attenuation properties should modify this second objective taking into consideration characteristics that improve attenuation over a range of frequencies. Some works in the literature have already begun to explore these new possibilities (Hussein et al. 2006) where both a performance metric and a design metric were considered for the second objective.

Another analysis that is more closely related with the constructive aspects can be made. From the point of view of the final implementation of this type of sonic barrier, the creation of vacancies following symmetries can play an important role. If it is supposed that structures with symmetry constraints are better in the productive process, Y and X symmetries can produce interesting results. For instance, in Fig. 9 it could be seen that points P4 and P5 of nosym3, P1 of symy3, and

P1 of symx3, produce quite similar solutions. In these cases, symmetries may be chosen if necessary for constructive purpose. Again, the multiobjective point of view offers a new perspective for obtaining satisfactory designs.

4 Conclusions

A new parallel multiobjective optimization algorithm has been developed and applied to a very difficult problem (optimization of SC attenuation properties by means of the creation of vacancies). A wide description of the algorithm is provided and a brief summary of its performances have been shown. This work also demonstrates that Multiobjective Optimization techniques, and in particular the ev-MOGA, can improve the acoustic properties of SCs made by two-dimensional arrays of rigid cylinders. The starting SC presents an average attenuation of 8.29 dB in the predetermined range of frequencies, and the best structure obtained, presents an average attenuation of 26.79 dB. These results show an a 300% improvement in the attenuation capability of the SC compared with starting SC. Parallelization of the ev-MOGA used here presents a significant time reduction and could be increased simply by adding new slave computers to the cluster.

With this new framework, future developments point to testing with new materials and/or new objective functions to take into account of, for example, attenuation in wider areas, and constructive requirements. New results that contribute a new multiobjective point of view have been obtained. The mean deviation of attenuation has demonstrated that it is not so important, and should be modified to achieve better attenuation properties.

All these developments have required a multidisciplinary team with sufficient expertise in different areas: evolutive optimization techniques and physical developments models for SCs.

References

Alander J (2002) An indexed bibliography of genetic algorithms & pareto and constrainedoptimization. Tech Rep, Dpt of Information Technology, University of Vaasa

Cantú-Paz E (1997) A survey of parallel genetic algorithms. Tech Rep 97003, Illimois Genetic Algorithms Laboratoty

Cervera F, Sanchis L, Sánchez-Pérez JV, Martínez-Sala R, Rubio C, Meseguer F, López C, Caballero D, Sánchez-Dehesa J (2002) Refractive acoustic devices for airborne sound. Phys Rev Lett 88:0239021–0239024

Chen Y, Ye Z (2001) Theoretical analysis of stop bands in two-dimensional periodic scattering arrays. Phys Rev E 64:036616

Coello C, Toscano G, Mezura E (2005) Information processing with evolutionary algorithms. In: Grana M, Duro R, d'Anjou A, Wang PP (eds) Information processing with evolutionary algorithms: from industrial applicationsto academic speculations. Springer, New York, pp 213–231

Coello C, Veldhuizen D, Lamont G (2002) Evolutionary algorithms for solving multi-objective problems. Kluwer, Dordrecht

Deb K (2007) Current trends in evolutionary multi-objective optimization. Int J Simul Multidiscipl Des Optim 1:1–8

Eshelman LJ (1991) The chc adaptive search algorithm: how to have safe search when engaging in nontraditional genetic recombination. In: Proceedings of the first workshop on foundations of genetic algorithms. Morgan Kaufmann, San Francisco, pp 265–283

Fonseca C, (1995) Multiobjective genetic algorithms with application to control engineeringproblems. PhD thesis, Dpt of Automatic Control and Systems Engineering, University of Sheffield

Fuster E, Romero-García V, García-Raffi LM, Sánchez-Pérez EA, Sopena M, Sánchez-Pérez JV (2006) A phenomenological model for sonic crystals based on artificial neural networks. J Acoust Soc Am 120(2):1–6

García-Pablos D, Sigalas M, de Espinosa FM, Torres M, Kafesaki M, García, N (2000) Theory and experiments on elastic band gaps. Phys Rev Lett 84:4349–4352

Gazonas GA, Weile DS, Wildman R, Mohan A (2006) Genetic algorithm optimization of phononic bandgap structures. Int J Solids Struct 43:5851–5866

Hakkansson A, Cervera F, Sánchez-Dehesa J (2005) Sound focusing by flat acoustic lenses without negative refraction. Appl Phys Lett 86:0541021–0541023

Herrero J, Blasco X, Martínez M, Ramos C, Sanchis J (2007) Non-linear robust identification of a greenhouse model using multi-objective evolutionary algorithms. Biosyst Eng 98(3):335–346

Herrero JM (2006) Non-linear robust identification using evolutionary algorithms. PhD thesis, Universidad Politécnica de Valencia, Valencia

Hussein MI, Hamza K, Hulbert GM, Saitou K (2007) Optimal synthesis of 2d phononic crystals for broadband frequency isolation. Waves Random Complex Media 17(4):491–510

Hussein MI, Hamza K, Hulbert GM, Scott RA, Saitou K (2006) Multiobjective evolutionary optimization of periodic layered materials for desired wave dispersion characteristics. Struct Multidisc Optim 31:60–75

Kafesaki M, Economou E (1999) Multiple scattering theory for three-dimensional periodic acoustic composites. Phys Rev B 60:11993

Kohn W, Rostoker N (1954) Solution of the schrodinger equation in periodic lattices with an aplication to metallic lithium. Phys Rev 94:1111

Korringa J (1947) On th calculation of the energy of a bloch wave in a metal. Physica XIII:392

Kushwaha M (1997) Stop-bands for periodic metallic rods: Sculptures that can filter the noise. Appl Phys Lett 70:3218–3220

Laumanns M, Thiele L, Deb K, Zitzler E (2002) Combining convergence and diversity in evolutionary multi-objective optimization. Evol Comput 10(3):263–282

Martínez-Sala R, Sancho J, Sánchez J, Gómez V, Llinares J, Meseguer F (1995) Sound attenuation by sculpture. Nature 378:241

Miettinen KM (1998) Nonlinear multiobjective optimization. Kluwer, Dordrecht

Mishra S, Deb K, Mohan M (2005) Evaluating the ϵ-domination based multi-objective evolutionary algorithm for a quick computation of pareto-optimal solutions. Evol Comput 13(4):501–526

Romero-García V, Fuster E, García-Raffi LM, Sánchez-Pérez EA, Sopena M, Llinares J, Sánchez-Pérez JV (2006) Band gap creation using quasiordered structures based on sonic crystals. Appl Phys Lett 88:1741041–17410413

Sánchez-Pérez JV, Caballero D, Martínez-Sala R, Rubio C, Sánchez-Dehesa J, Meseguer F, Llinares J, Gálvez F (1998) Sound attenuation by a two-dimensional array of rigid cylinders. Phys Rev Lett 80:5325–5328

Sánchez-Pérez JV, Rubio C, Martínez-Sala R, Sánchez-Grandia R, Gómez V (2002) Acoustic barriers based on periodic arrays of scatterers. Appl Phys Lett 27:5240–5242

Sanchis L, Hakkansson A, López-Zanón D, Bravo-Abad J, Sánchez-Dehesa J (2004) Integrated optical devices design by genetic algorithm. Appl Phys Lett 84:4460–4462

Shen M, Cao W (2001) Acoustic band-gap engineering using finite-size layered structures of multiple periodicity. Appl Phys Lett 75:3713–3715

Sigalas M, Economou E (1992) Elastic and acoustic wave band structure. J Sound Vib 158:377

Zitzler E (1999) Evolutionary algorithms for multiobjective optimization: Methods and applications. Ph.D. thesis, Swiss Federal Institute of Technology Zurich